Quantifying in-situ gas hydrates at active seep sites in the eastern Black Sea using pressure coring technique

K. Heeschen[1,*], M. Haeckel[2], I. Klaucke[2], M. K. Ivanov [3], and G. Bohrmann[1]

[1]{Research Centre Ocean Margins, Bremen, Germany}

[2]{Leibniz Institute of Marine Sciences (IFM-GEOMAR), Kiel, Germany}

[3]{M.V. Lomonosov Moscow State University, Moscow, Russia}

[*]{now at: Federal Institute for Geosciences and Natural Resources (BGR), Hannover, Germany}

Correspondence to: K. Heeschen (katja.heeschen@bgr.de)

Abstract

In the eastern Black Sea, we determined methane (CH_4) concentrations, gas hydrate volumes and their vertical distribution from combined gas and chloride (Cl^-) measurements within pressurized sediment cores. The total gas volume collected from the cores corresponds to concentrations of 1.2 – 1.4 mol/kg CH_4 at in-situ pressure, which is equivalent to a gas hydrate saturation of 15 – 18% of pore volume and amongst the highest values detected in shallow seep sediments. At the central seep site, a high-resolution Cl^- profile resolves the upper gas hydrate stability boundary and a continuous layer of hydrates in a sediment column of 120 cm thickness. Including this information, a more precise gas hydrate saturation of 22 – 24% pore volume can be calculated. This is higher in comparison to a saturation calculated from the Cl^- profile alone, resulting in 14.4%. The likely explanation is an active gas hydrate formation from CH_4 gas ebullition. The hydrocarbons at Batumi Seep are of shallow biogenic origin (CH_4 > 99.6%), at Pechori Mound they originate from deeper thermocatalytic processes as indicated by the lower ratios of C_1 to C_2-C_3 and the presence of C_5.

1 Introduction

Gas hydrates consist of water cages enclosing methane (CH_4) as the major guest molecule (Sloan and Koh, 2007). Given that pore fluids are saturated with CH_4, gas hydrates form at high pressure and low temperature conditions common at ocean depths exceeding 300 – 500 m (Sloan and Koh, 2007). Because of the difficulties to inventory marine gas hydrates, considerable controversy remains about the amount and distribution of gas hydrates in marine sediments, and thus their potential as an energy resource or a contributor to past and future climate changes (e.g., Milkov, 2005).

Inventory uncertainties arise from the loss of gas during core recovery, crude sampling resolution, and/or uncertain calibration of indirect methods such as acoustic detections (Dickens et al., 1997;Milkov, 2005). Porewater chloride (Cl^-) anomalies are frequently used to estimate gas hydrate volumes. This is based on the exclusion of salt from the hydrate crystal lattice during hydrate formation in the sediment and the respective fresh water release when decomposition is initiated during core recovery, resulting in negative Cl^- anomalies where gas hydrates had been present (e.g., Haeckel et al., 2004). However, small scale distributional variations, non-steady state conditions, and brine formation in hydrate voids contribute to estimate uncertainties as do variations of Cl^- caused by the advection of less saline fluids from depth (Haeckel et al., 2004). Pressure cores were developed within the ODP/IODP program (Dickens et al., 1997) and for coring of surface sediments (Abegg et al., 2008;Heeschen et al., 2007). They allow for determining the sediment's total in-situ CH_4 inventory that is present as hydrate-bound, gaseous and dissolved CH_4. This inventory then allows the calculation of the gas hydrate volume based on stability conditions and the equation of state.

Here we compare gas hydrate inventory estimates using two methods: the collection of gas from pressurized sediment cores and porewater chloride anomalies measured on the same cores. The samples originate from recently discovered seep sites off Georgia in the eastern Black Sea (Akhmetzhanov et al., 2007;Bohrmann et al., 2007). Despite gas hydrate discoveries in this area (Klauke et al., 2006;Pape et al., 2010) little is known about gas hydrate distributions and regional quantities in the Black Sea, the largest anoxic basin at present times (Ross and Degens, 1974). Our results indicate that the gas hydrate volumes are amongst the highest in seep surface sediments worldwide.

2 Geological Setting

The Black Sea is an extensional basin with organic-rich sediments of varying salinity and a total of 12 – 16 km thickness. This stack includes the thick clay-rich Maikopian Unit (Ross and Degens, 1974), which is the source of frequent mud diapirism (Ross and Degens, 1974;Wagner-Friedrichs, 2007). Seep sites with CH_4 gas ebullition and fluid flow are common in the Black Sea basin and lead to very high CH_4 concentration in the anoxic bottom waters (Reeburgh, 2007) and widely distributed gas hydrate occurrences in the sediments (Vassilev and Dimitrov, 2002). Large numbers of gas seeps have also been discovered in the south eastern Black Sea (Klauke et al., 2006), which is characterized by severe faulting and slumping (Ross and Degens, 1974).

Batumi (water depth: 850 m) and Pechori seeps (1000 m) are located on the Kobuleti Ridge, a complex canyon-ridge system (Fig. 1) where buried diapiric structures and fault systems form migration pathways for sediments, fluids and gases (Wagner-Friedrichs, 2007). The Batumi seep area is the largest seep site with an areal extent of 0.5 km^2 characterized by shallow gas hydrates, authigenic carbonates, and vigorous gas venting (Klauke et al., 2006;Pape et al., 2010). Pechori Mound has 75 m of relief, steep slopes, and strong seafloor reflection at the top (Wagner-Friedrichs, 2007). It is rich in oil and massive gas hydrates. Indications for structure I gas hydrate, i.e., gas hydrates with CH_4 as the prevailing guest molecule, were found at both sites (Pape et al., 2010; S. Klapp, Univ. Bremen, pers. comm., 2008).

3 Methods

The sediment cores originate from pressure coring operations using the Dynamic Autoclave Piston Corer (DAPC) (Abegg et al., 2008) on board RV Logachev (Akhmetzhanov et al., 2007), cruise TTR-15 (Tab. 1). The cores were degassed on board and subsequently sampled for porewater fluids.

3.1 Pressure coring, gas collection and volume calculations

The DAPC recovers a sediment core of up to 2.3 m length at in-situ pressure using a newly developed enhanced pressure-preserving system. Once on board, its pressure chamber is fixed upright, cooled in an ice-bath and linked to a pressure sensor, an assembly of gas-tight valves for gas sub-sampling, and a volumetric plastic cylinder that allows the measurement of

released water and gas volumes. For details: (Heeschen et al., 2007). The main degassing takes several hours and is stopped when gas bubbling has ceased for several tens of minutes. When the core has warmed to ambient temperature, it is reopened to collect the small amounts of residual exsolved gas.

The gas samples were analyzed with an Agilent gas chromatograph for hydrocarbons C_1 - C_5 (FID) and for oxygen, nitrogen and CO_2 (TCD). Standards were: 100% C_1, C_2, C_3 and CO_2, bottled mixtures of 100 ppm and 1000 ppm C_1 through C_5 standards (in nitrogen), and air. The precision of standard measurements was 3%. Contaminations of the core gas with air was measured ($\Sigma O_2 + N_2$; 2 – 2.5%, Tab. 2) and subtracted. The hydrocarbon gas compositions are given in percentage of the sum of hydrocarbon gases (% $\Sigma C_{1\text{-}5}$, hereafter cited as %). The accuracy of the total gas volumes (gas / L; Tab. 2) is generally 5%. For details: (Heeschen et al., 2007).

All dissolved, free, and hydrate-bound CH_4 (ΣCH_4 / mol) is released and collected from the core during its controlled degassing. To calculate the porewater CH_4 in-situ concentration (Tab. 2; CH_4 / mol/kg), ΣCH_4 is related to the amount of porewater present between the bottom of the core and the sulfate depletion depth, assuming an even distribution throughout this depth range (Heeschen et al., 2007). Assuming dissolved and hydrate-bound CH_4 to be present, we subtract the saturation concentration (c_{eq}) of 0.087 mol/kg of CH_4 (Tishchenko et al., 2005; also see Appendix A) before calculating gas hydrate volumes. The molar CH_4/water ratio for the structure I gas hydrates is assumed to be 5.9, a value that was observed in natural structure I gas hydrates with an occupancy of 90% of small cages by CH_4 (Ussler and Paull, 2001). All gas volumes refer to STP conditions (1 bar and 25 °C), resulting in a CH_4 volume of 182 L per liter of gas hydrate.

3.2 Gas hydrate and porewater analysis

The gas hydrates were recovered with TV-grab (TVG) or gravity corer (GC). Clean samples were put into headspace vials that were sealed by crimping, and vented into a second vial by a vacutainer. The gas was analyzed on board (see 3.1).

The sediment of DAPC cores was sampled for porewater. In case of core BS351AP1 the entire core was cut into 5 cm thick slices. Porewater was extracted using a low-pressure squeezer (<5 bar; 8°C; 0.2 µm cellulose acetate Nuclepore filters) and analysed for SO_4^{2-} and Cl^- using ion chromatography and Mohr titration, respectively (Wallmann et al., 2006 and references

therein). IAPSO seawater standard was used for calibration. Precision of the Mohr titration is in the range of ±10 mM Cl^-. The porosity listed in Tab. 1 was determined by weight difference, before and after freeze-drying. For the conversion into volume ratio (volume of porewater/volume of bulk sediment) we apply a dry sediment density of 2.5 g/cm^3 (Haeckel et al., 2004) and a Black Sea water density of 1.021 g/cm^3.

The core depths of BS351AP are corrected for the loss of surface sediments caused by the heavy coring gear using porosity data from video guided multi core sampling at the same geographical coordinates (Table 1, Appendix A).

3.3 Modeling the chloride anomaly for its relation to the hydrate content

Observed Cl^- anomalies can be converted to an amount of gas hydrate in percent of the pore volume (GH / %pv) using:

$$GH = \frac{\Delta Cl}{Cl_{ref}} \frac{\rho_{PW}}{\rho_{GH}} \frac{M_{GH}}{M_{H2O}} \frac{1}{x_{H2O}} \quad (1)$$

where ΔCl = deviation of measured Cl^- concentration from in-situ value (Cl_{ref}), ρ_{PW} = density of porewater, ρ_{GH} = density of natural hydrate, M_{GH} = molecular weight of methane hydrate, M_{H2O} = molecular weight of water, and x_{H2O} = molar ratio of water/methane for natural gas hydrate (Tab. S1). A numerical 1-D transport-reaction model (Haeckel et al., 2004) was applied to provide the theoretical in-situ Cl^- concentration profile (Cl_{ref}). See Appendix for details on the model.

4 Results and Discussion

4.1 Highest CH_4 concentrations in shallow anoxic seep sediments

Most of the in-situ CH_4 concentrations in shallow sediments of the eastern Black Sea seeps (Tab. 2) considerably exceed values determined from pressurized cores taken in equivalent environments elsewhere (Heeschen et al., 2007). Maximum gas volumes occurred at sites of very high backscatter intensity at Batumi Seep (BS378AP, 200 L and BS351AP, 226 L) (Fig. 1). The shorter core, BS371AP, was taken slightly to the NE and had a smaller gas volume (11 L). At the central high backscatter zone of Pechori Mound core BS359 contained 88 L.

The ~~large~~ gas volumes from the high reflectivity zones ~~relate~~ to consistent in-situ CH_4 concentrations of 1.2 – 1.4 mol/kg porewater at depths below sulfate penetration (Tab. 2). These CH_4 concentrations are ~ 30% higher than those of surface seep sediments from the gas hydrate stability zone in the Gulf of Mexico and the Anaximander Mountains (Mediterranean Sea) where maximum in-situ CH_4 concentrations were about 1 mol/kg (Heeschen et al., 2007). Concentrations from conventional and pressurized coring differ by two orders of magnitude at all sites caused by loss of CH_4 during core retrieval. For example, at Batumi Seep, maximum CH_4 concentrations of 0.013 mol/kg were measured in conventional cores (Klauke et al., 2006). This is despite the visual observations of gas hydrates and a calculated CH_4 saturation (c_{eq}) of 0.087 mol/kg in the presence of gas hydrates at the site.

All in-situ CH_4 concentrations are ~~far~~ above saturation. The excess CH_4 ($>c_{eq}$) is bound in gas hydrate, which at three out of four sites occupies a rather consistent pore volume of ~16.5% (% pv) or a core volume of 12% (% cv) at ~~any~~ depth between the sulfate penetration and the core bottom (Tab. 2, Fig. 2a). For better comparison with published data we refer to % pv hereafter. Core BS371AP from the area of intermediate backscatter intensity ~~still holds~~ 2% pv of gas hydrate~~s~~.

Despite the low fluid advection rates at Batumi Seep of 0.1 cm a^{-1} (see Appendix A), the gas hydrate volumes are slightly higher than the average of 5 – 15% pv estimated for high fluid flow sites (Milkov, 2005). It is therefore likely that the strong gas hydrate formation is fueled by the vigorous gas ebullition observed in the area (Klauke et al., 2006;Pape et al., 2010). This inference further supports earlier calculations (Haacke et al., 2009;Haeckel et al., 2004), requiring free gas transport for the formation of high amounts of near-surface gas hydrates.

4.2 Gas hydrate distribution from chloride measurements

The degassing of DAPC cores holds no information on the vertical distribution of gas hydrates in the sediment as do high-resolution Cl^- profiles commonly used on conventional cores to determine the gas hydrate distribution and quantities. ~~The main argument against the~~ latter application is the assumption of a linear background Cl^- profile, ~~thus potentially ignoring~~ the possibility of local Cl^- enrichments from recent gas hydrate formation (Haeckel et al., 2004) and the presence of brines or free gas in gas hydrate voids (Milkov et al., 2004).

To compare two methods of gas hydrate budgeting ~~and use respective advantages~~, we ~~established~~ a high-resolution Cl^- profile in the gas-rich core, BS351AP, from Batumi Seep

after degassing (Fig. 2b and 2c). At the seep two processes lower the Cl^- concentration: 1) the upward-directed transport of Cl-depleted fluids from deeper limnic sediments (Ross and Degens, 1974) ~~that induces linearly decreasing background Cl^- concentrations with depth~~ and 2) local gas hydrate decomposition, which ~~leads to irregular Cl^- excursions from the baseline~~. ~~Combining the~~ high-resolution Cl^- profile from BS351AP and 1-D numerical transport-reaction modeling ~~is clearly able to~~ resolve both processes (Fig. 2b and 2c, Appendix A)~~.~~ ~~Whereas~~ transport ~~processes~~ determine the background ~~concentrations~~ (dotted line), ~~the~~ decomposition of gas hydrates leads to a broad diversion (solid line) at 85 – 205 cm (depth corrected, Table 1) plus comparably small diversions at 75 and 225 cm~~, both of them~~ within the precision of the Cl^- measurements. Calculations using the major Cl^- anomaly between 85 – 205 cm core depth result in a mean in-situ CH_4 concentration of 1.04 mol/kg in this depth range. This is equivalent to an average gas hydrate volume of 14.4% pv containing 125 L of CH_4 gas (at STP). Including the possible Cl^- anomalies above and below the interval of 85 – 205 cm, the total gas volume is 140.7 L, thus indicating that at most 12% of gas may originate from depths beyond 85-205 cm.

~~From the Cl^- profile it becomes clear that nearly all gas hydrate is present~~ at 85 – 205 cm. If the CH_4 inventory gained from core degassing is corrected for this true depth range of gas hydrate occurrences, the degassed CH_4 volume relates to an average CH_4 concentration of 1.945 mol/kg and a gas hydrate occupancy of 24% pv in a layer with a thickness of 120 cm (Fig 2, Tab. 2: $BS351AP^{85\text{-}205cm}$). Assuming that a maximum of 12% of collected gas is located at other depths this occupancy relates to 22% pv (Fig 2, Tab. 2: $BS351AP^{85\text{-}205,88\%}$). This is 7 – 10% above the value from Cl-based calculations.

The disparity between the methods can be explained by ~~active formation of hydrates and non-steady state conditions producing significant in-situ Cl^- enrichments.~~ ~~These~~ cannot be accounted for with a steady state model, nor can they be resolved in porewater profiles of retrieved cores as they are overprinted by ~~A) the freshening due to~~ gas hydrate decomposition during core recovery (and degassing procedure) ~~and~~ ~~B)~~ dilution ~~due to diffusive~~ and, ~~particularly,~~ advective mixing with the lower chloride concentrations in the surrounding porewater (Haeckel et al., 2004) (Appendix A). It is unlikely ~~that~~ the disparity is caused by ~~the presence of a substantial amount of~~ free gas, i.e. not bound in gas hydrates. During degassing free gas ~~would be~~ released first, while gas hydrates ~~are still~~ stable. ~~It~~ would be enriched in gas molecules excluded from gas hydrate formation or be similar to the advecting

vent gas if caused by ebullition. In core BS351AP, ~~only~~ the first 11 L of the released gas ~~have a slightly different gas composition~~ with ethane (C_2) ~~being enriched~~ (Appendix B). However, this volume would only account for 0.5% of the gas hydrate volume, i.e., a small fraction of the disparity.

Our approach of combining both methods provides the means to greatly improve the quantification of sedimentary hydrate contents via pressure coring. While the degassing of pressurized cores resolves quantities and gas compositions, the Cl^- profile holds information about the vertical gas hydrate distribution and determines gas hydrate stability conditions (Heeschen et al., 2007;Milkov et al., 2004). Further, a discrepancy between both methods is a good indicator for recent and ongoing gas hydrate formation.

4.3 Gas compositions derived from pressure coring

The composition of the gas released from the DAPC cores consists of hydrocarbons (98%) and small contaminations of air of 2 – 2.5 % (Tab. 2), which we subtracted. At Batumi Seep the released hydrocarbons (Σ_{C1-C5}) consist of 99.63% CH_4, a small contribution of ethane, and traces of propane, whereas at Pechori Mound C_2 and C_3 compositions are one order of magnitude higher and C_{4+} are present (Tab. 3). CH_4 and C_2 can be produced through both, the microbial (biogenic) and thermocatalytic (thermogenic) decomposition of organic matter, whereas C_{3+} alkanes are mainly assigned to thermocatalytic reactions at greater depth (Whiticar, 1999). The ratio of methane to ethane and propane, called the Bernard ~~Factor~~ ($B_f = CH_4/(C_2+C_3)$) is used to distinguish between biogenic and thermogenic pathways for alkane gases (Whiticar, 1999). Batumi Seep displays B_f-values of 2700 – 3800, indicating a largely biogenic origin, which is in good agreement with data from (Pape et al., 2010). At Pechori Mound, however, a B_f of 400 and the presence of C_{4+} and oil strongly supports a thermogenic origin of the gas.

These geochemical inferences are in good agreement with those from visual and seismic observations. At Batumi Seep a wide feeder channel and/or diapiric structure allowing transport of material from greater depth is absent (Wagner-Friedrichs, 2007). Instead, an array of near vertical faults is present, some of them penetrating a bottom simulating reflector at ~150 mbsf and reaching the seafloor (Wagner-Friedrichs, 2007). This supports major contributions of shallow biogenic gas. At Pechori Mound observations from seismic data indicate that gas-rich sediments and fluids rise through a structure-wide feeder channel that is

connected to a diapir below (Wagner-Friedrichs, 2007), which is probably composed of the organic-rich Maikopian Formation, found elsewhere at 1000 – 4000 m sediment depth (Meredith and Egan, 2002). Assuming a general geothermal gradient of 30 ˚C/km, the temperature range in the shallower part of these strata is well within the gas production window of 120 – 220 ˚C (Tissot and Welte, 1984). In accordance with these indications, the porewater analysis of Li, B, $\delta^{18}O$ and $^{87/86}Sr$ propose a fluid source at higher temperatures (>100 ˚C) from smectite-illite transformation only at Pechori Mound (Reitz et al., subm).

The difference in gas compositions at the two sites is strongly expressed in the gas hydrate composition (Tab. 4). Whereas gas hydrates at Batumi Seep contain C_1 and C_2 only, the hydrate samples from Pechori Mound have a C_2/C_3 ratio <1, often characteristic for a mixture of gas hydrate structures (Sloan and Koh, 2007). Pure methane hydrates were reported earlier at Batumi Seep (Klauke et al., 2006;Pape et al., 2010).

5 Conclusions

Combined measurements of gas volumes and high-resolution porewater chlorinity on pressurized cores allow assessing gas hydrate volumes, formation, distribution and origin. At sites in the Eastern Black Sea gas hydrate volumes in shallow sediments are among the highest values known worldwide with up to 24% pv, exceeding average known values by 10% pv. Further investigations will test whether these high gas hydrate volumes represent a local enrichment or are widely distributed in the organic-rich sediments of the anoxic Black Sea. The investigated gas hydrates at the central Batumi Seep occurred mostly at 85 – 205 cm depth and differences between the chloride-based (140.7 L) and the collected (211 L) CH_4 gas volume indicates currently active gas hydrate formation not to be resolved from porewater data. ~~Pure methane hydrates at Batumi Seep are fed by the ebullition of biogenic CH_4 gas, whereas at Pechori Mound light hydrocarbons originate from the advection of fluids enriched in thermogenic hydrocarbons and oil.~~

Appendix A: Numerical transport-reaction modelling

A simple 1-D transport-reaction model (Haeckel et al., 2004) was adopted to simulate the observed Cl^- data and the corresponding methane hydrate formation. Four chemical species

(chloride, methane, sulfate, and gas hydrate) and the porosity change due to hydrate formation were considered.

A 1.1 Model description

A 1.1.1 Porosity

In early diagenetic models the porosity depth distribution, $\phi(x)$, generally does not change significantly with time, and hence, is prescribed by an empirical function fitted to the measured porosity data (Fig. S1). Gas hydrate formation reduces the porosity with time. Thus, porosity was calculated using:

$$\phi(x,t) = \phi_\infty + (\phi_0 - \phi_\infty)e^{-\beta x} - GH(x,t) \quad \text{(A1)}$$

where ϕ_0=porosity at the sediment surface (x=0), ϕ_∞=porosity at infinite depth (x=∞), and GH=porosity reduction due to gas hydrate.

The 'true' porosity of hydrate-bearing, near-surface sediments results from a combination of hydrate pieces, gas hydrates filling pore spaces, and hydrate-free sediments. In addition, hydrate pieces displace the original sediment, thus producing fractures. Despite an internal porosity close to zero, they do not seal the sediment above the hydrate layer from that below because the pieces are intercalated in the sediment matrix. This complex mechanism needs future investigation before 'true' porosity calculations are feasible. For now, we approximate the porosity reduction as if hydrate formation is solely filling the pore space. We are confident that this description leads only to small errors in our results.

A1.1.2 Advection

Assuming steady state compaction, the burial velocity can be expressed as:

$$w(x,t) = \frac{1-\phi_\infty}{1-\phi(x,t)} w_\infty \quad \text{(A2)}$$

where w_∞= sedimentation rate at infinite depth.

Since burial and compaction at cold vent sites are much smaller than the upward fluid flow, they can be neglected and the advection rate is:

$$u(x,t) = \frac{\phi_0}{\phi(x,t)} u_0 \quad \text{(A3)}$$

where u_0=fluid flow rate at the sediment surface.

A1.1.3 Methane hydrate formation

Methane hydrate formation is assumed proportional to the saturation state of methane in the porewater with respect to its equilibrium concentration in the presence of the hydrate phase (L_{GH}):

$$R_{GH} = k_{GH}(\frac{CH_4}{L_{GH}} - 1) \quad \text{(A4)}$$

L_{GH} was calculated following (Tishchenko et al., 2005). The kinetic constant k_{GH} has units of volume hydrate by bulk sediment volume and time. Hydrate formation is simulated within the entire modeled sediment column.

Since hydrate formation withdraws methane from the porewater, the rate of methane consumption (in units of mole CH_4 per volume porewater and time) is related to R_{GH} by:

$$R_M = \frac{\rho_{GH}}{M_{GH}\phi} R_{GH} \quad \text{(A5)}$$

where ρ_{GH}=density of methane hydrate and M_{GH}=molar weight of natural gas hydrate.

A1.1.4 Methane gas dissolution

As gas bubbles rise through the sediments they are replenishing the porewater methane content. A first order rate accounts for this dissolution of ascending gas bubbles:

$$R_{MB} = k_{MB}(L_{MB} - CH_4) \quad \text{(A6)}$$

where methane concentration in equilibrium with the gas phase, L_{MB}, is calculated following (Tishchenko et al., 2005). Methane gas is represented by a source term for methane dissolved in the porewater (Eq. A6,

(A15). It is not transported explicitly by the model. L_{GH} and L_{MB} are kept constant during the model runs because the imposed salinity change does not alter the methane equilibrium concentrations significantly enough to affect the model results. Additionally, pressure and temperature are constant in the investigated sediment interval.

Finally, based on ROV observations of vigorous ebullition of methane gas bubbles at the seafloor, we believe that the assumption of an inexhaustible methane gas source is justified.

A1.1.5 Anaerobic oxidation of methane (AMO)

As additional reaction affecting dissolved methane concentrations, anaerobic methane oxidation (AMO) was included:

$$CH_4 + SO_4^{2-} \rightarrow HCO_3^- + HS^- + H_2O \quad \text{(A7)}$$

Mathematically, a second-order rate law describes this redox reaction:

$$R_{AMO} = k_{AMO}\ CH_4\ \ SO_4^{2-} \quad \text{(A8)}$$

where k_{AMO} is the rate constant for AMO.

A1.1.6 Chloride exclusion

During methane hydrate formation chloride is excluded from the hydrate phase and added to the surrounding porewater. This mass change of porewater over time can be expressed as:

$$m_{PW}^f = m_{PW}^i - dm_{GH} \quad \text{(A9)}$$

where the indices *i* and *f* denote the mass of porewater before and after hydrate formation and dm_{GH} is the mass of the precipitated gas hydrate. Converting mass into a volume balance leads to:

$$V_{PW}^f = V_{PW}^i - \frac{\rho_{GH}}{\rho_{PW}} dV_{GH} \quad \text{(A10)}$$

Thus, the change in chloride concentration, *dCl*, can be written:

$$dCl = Cl^f - Cl^i = \frac{n_{Cl}^f}{V_{PW}^i - \frac{\rho_{GH}}{\rho_{PW}} dV_{GH}} - Cl^i = \frac{n_{Cl}^i}{V_{PW}^i - \frac{\rho_{GH}}{\rho_{PW}} dV_{GH}} - Cl^i \quad \text{(A11)}$$

where n_{Cl}=amount of chloride before (*i*) and after (*f*) hydrate formation, and n^f_{Cl}=n^i_{Cl}, since the total mass of chloride remains constant during hydrate formation. Rearranging gives:

$$dCl = \frac{Cl^i \rho_{GH} dV_{GH}}{\rho_{PW} V_{PW}^i - \rho_{GH} dV_{GH}} = \frac{Cl^i \rho_{GH} dGH}{\rho_{PW} \phi^i - \rho_{GH} dGH} \quad \text{(A12)}$$

where porosity $\phi = V_{PW}/V_{bulkSed}$ and $dGH = dV_{GH}/V_{bulkSed}$ is porosity change due to methane hydrate formation. The rate of chloride exclusion ($R_{Cl} = dCl/dt$) is related to the hydrate formation rate ($R_{GH} = dGH/dt$) by:

$$R_{Cl} = \frac{dCl}{dt} = \frac{Cl \rho_{GH}}{\rho_{PW} \phi - \rho_{GH} dGH} R_{GH} \approx Cl \frac{\rho_{GH}}{\rho_{PW} \phi} R_{GH} \quad \text{(A13)}$$

where the simplification holds when $\rho_{GH}\, dGH << \rho_{PW}\, \phi$ for small dt.

A1.1.7 Model equations

The model's governing transport-reaction equations are:

Chloride: $$\frac{\partial \phi Cl}{\partial t} = \frac{\partial}{\partial x}\left(\phi \frac{D_{Cl}}{\theta^2} \frac{\partial Cl}{\partial x} + \phi_0 u_0 Cl \right) + Cl \frac{\rho_{GH}}{\rho_{PW}} k_{GH} \left(\frac{CH_4}{L_{GH}} - 1 \right) \quad \text{(A14)}$$

Methane: $$\frac{\partial \phi CH_4}{\partial t} = \frac{\partial}{\partial x}\left(\phi \frac{D_{CH_4}}{\theta^2} \frac{\partial CH_4}{\partial x} + \phi_0 u_0 CH_4 \right) - \frac{\rho_{GH}}{M_{GH}} k_{GH} \left(\frac{CH_4}{L_{GH}} - 1 \right) + \phi k_{MB} (L_{MB} - CH_4) - \phi\, k_{AMO} SO_4^{2-} CH_4 \quad \text{(A15)}$$

Gas hydrate: $$\frac{\partial GH}{\partial t} = -\frac{1 - \phi_\infty}{1 - \phi} w_\infty \frac{\partial GH}{\partial x} + k_{GH} \left(\frac{CH_4}{L_{GH}} - 1 \right) \quad \text{(A16)}$$

Sulfate: $$\frac{\partial \phi SO_4^{2-}}{\partial t} = \frac{\partial}{\partial x}\left(\phi \frac{D_{SO_4^{2-}}}{\theta^2} \frac{\partial SO_4^{2-}}{\partial x} + \phi_0 u_0 SO_4^{2-} \right) - \phi\, k_{AMO} SO_4^{2-} CH_4 \quad \text{(A17)}$$

where D_i=diffusion coefficients of Cl^-, CH_4, and SO_4^{2-} corrected for salinity, temperature and pressure (Hayduk and Laudie, 1974;Li and Gregory, 1974), and $\theta^2 = 1 - 2\ln\phi$ is the tortuosity correction for diffusion (Boudreau, 1997).

This set of partial differential equations was solved numerically within the MATLAB® environment. The discretization of Eqs. A14-A17 was done using finite differences and a combination of Dirichlet and Neumann boundary conditions (see Tab. S1 for details). The initial conditions are based on the steady state profiles of the "no gas hydrate" condition: (i)

linearly decreasing Cl^- concentrations with depth, (ii) methane and sulfate profile if only anaerobic methane oxidation is present and in equilibrium with methane gas phase, (iii) no gas hydrate, and (iv) observed porosity profile.

Five parameters were adjusted by comparing the model result with the observed data: (i) the advection rate (u_0), (ii) the rate constant for hydrate formation (k_{GH}), (iii) the rate constant for gas bubble dissolution (k_{MB}), (iv) the rate constant for anaerobic methane oxidation (k_{AMO}), and (v) the simulation time (t_{max}).

A 1.2 Model results

A sensitivity analyses was performed to constrain the values of these five fit parameters. The best fit (Fig. S1) to the observed data was achieved for low fluid advection velocities (u_0 = 0.1 cm/a) as the measured chloride profile does not show significant curvature, except for the hydrate related anomaly. The rate constant for anaerobic methane oxidation (k_{AMO}) basically influences the increase in sedimentary hydrate content near the surface because AMO competes with hydrate formation for the available dissolved methane. A minimum AMO rate constant of k_{AMO}=0.03 mM^{-1} a^{-1} is able to resemble a steep increase as it can be inferred from the measured Cl anomaly. Diffusion of methane from below is only able to form very little gas hydrate. In order to build up considerable amounts of hydrate (i.e., several %pv) an additional methane source is needed. Therefore methane gas bubble dissolution has been included in the model. This process is also required in order to deliver enough methane to the surface sediments, so that the onset of hydrate formation at a sediment depth of ~85 cm can be resembled (see start of observed Cl anomaly in Fig. S1). The predicted rate constant for methane gas bubble dissolution is k_{MB}=0.2 a^{-1}. To balance this increased methane flux to the porewater and keep dissolved methane concentrations at equilibrium with the hydrate phase (L_{GH}=87 mM, see Tab. S1), hydrate formation needs to proceed with a rate constant of at least k_{GH}=0.005 a^{-1}. Finally, a simulation time of several hundreds of years (i.e., here 500 a) ensures that the modeled solute concentrations (Cl^-, CH_4, and SO_4^{2-}) are at steady state; the solid gas hydrate profile is, of course, not at steady state after this time. For a simulation time of 500 years, the model predicts an average hydrate concentration of 15.2% pv. This is in good agreement with the amount calculated from the chloride anomaly (14.4% pv), but 10% less than the amount derived from the degassing method (25% pv). However, it is difficult to

conclude an age of the Batumi Seep area from this finding, because hydrate related seeps are dynamic systems and methane fluxes can vary over time by orders of magnitude. In contrast, the model simulation assumes a constant methane flux and a constant hydrate formation rate over the entire simulation time.

A2. Degassing characteristics core BS351AP

Methane is the main constituents of the gas collected from pressure core BS351AP with small contributions of ethane and traces of propane and i-pentane (Figure S2.1). Their ratios vary only slightly (< 0.01%). The more significant alterations occur at the beginning and in the end of the degassing. At the start of the degassing this may relate to free gas, gas hydrate of slightly different composition or ethane originating from the pore water. Free gas should be released immediately, except volumes are small and caught in the gas hydrate layer where pathways are blocked until gas hydrates start to decompose and overpressure is strong. This process might also explain the spike occurring at about 120 L. At this point opening pathways could have released a minor amount of overpressurised and encased gas leading to the pressure drop in the volume-pressure plot. Pore water degassing should release constituents that are excluded from gas hydrate structure I cages, such as i-pentane, which is clearly increasing during the last stage of the degassing, indicating pore water to degas but not during the early degassing. There should be no differences in gas hydrate stability given any of the occurring compositions; therefore only one threshold pressure is present.

Acknowledgements

Our special thanks go to: H.-J. Hohnberg, F. Abegg, B. Domeyer, K. Nass M. Bausch, M. Reuschel, P. Behrend, the master and crew of RV Logachev and the TTR-15 onboard party. We are very thankful for the very constructive reviews of Walter S. Borowski on an earlier version of the manuscript. Financial support was granted by the German Research Foundation, the German Ministry of Education and Research (project METRO, 03G0604A). This is publication GEOTECH-?? of R&D program GEOTECHNOLOGIEN, RCOM publication No.??

References

Abegg, F., Hohnberg, H.-J., Pape, T., Bohrmann, G., and Freitag, J.: Development and application of pressure-core-sampling systems for the investigation of gas- and gas-hydrate-bearing sediments, Deep Sea Research Part I, 55, 1590-1599, 2008.

Akhmetzhanov, A. M., Ivanov, M. K., Kenyon, N. H., Mazzini, A., and Cruise participants: Deepwater cold seeps, sedimentary environments and ecosystems of the Black and Tyrrhenian Seas and Gulf of Cadiz, UNESCO, 99, 2007.

Bohrmann, G., Pape, T., and Cruise participants: Report and preliminary results of R/V Meteor cruise M72/3, Istanbul–Trabzon–Istanbul, 17 March – 23 April, 2007. Marine gas hydrates of the Eastern Black Sea, University of Bremen, Bremen, 2007.

Boudreau, B. P.: Diagenetic Models and Their Implementation: Modelling Transport and Reactions in Aquatic Sediments, Springer-Verlag, Berlin, Heidelberg, New York, 414 pp., 1997.

Dickens, G. D., Paull, C. K., Wallace, P., and Party, O. L. S.: Direct measurement of in situ methane quantities in a large gas-hydrate reservoir, Nature, 385, 426-428, 1997.

Haacke, R. R., Hyndman, R. D., Park, K. P., Yoo, D. G., Stoian, I., and Schmidt, U.: Migration and venting of deep gases into the ocean through hydratechoked chimneys offshore Korea, Geology, 37, 531-534, 2009.

Haeckel, M., Suess, E., Wallmann, K., and Rickert, D.: Rising methane gas bubbles form massive hydrate layers at the seafloor, Geochimica and Cosmochimica Acta, 68, 4335-4345, 2004.

Hayduk, W., and Laudie, H.: Prediction of diffusion coefficients for nonelectrolytes in dilute aqueous solutions, American Institute of Chemical Engineers Journal, 20, 611-615, 1974.

Heeschen, K. U., Hohnberg, H.-J., Abegg, F., Drews, M., Haeckel, M., and Bohrmann, G.: In-situ hydrocarbon inventory from pressurized cores in surface sediments, Northern Gulf of Mexico, Marine Chemistry, 107, 498-515, 2007.

Klauke, I., Sahling, H., Weinrebe, W., Blinova, V., Bürk, D., Lursmanashvili, N., and Bohrmann, G.: Acousitc investigation of cold seeps offshore Georgia, eastern Black Sea, Marine Geology, 231, 51-67, 2006.

Li, Y.-H., and Gregory, S.: Diffusion of ions in sea water and in deep-sea sediments, Geochimica et Cosmochimica Acta, 38, 703-714, 1974.

Meredith, D. J., and Egan, S. S.: The geological and geodynamic evolution of the eastern Black Sea basin: insights from 2-D and 3-D tectonic modelling, Tectonophysics, 350, 157-179, 2002.

Milkov, A. V., Dickens, G. D., Claypool, G. E., Lee, Y. J., Borowski, W. S., Torres, M. E., Xu, W., Tomaru, H., Tréhu, A. M., and Schultheiss, P.: Co-existence of gas hydrate, free gas, and brine within the regional gas hydrate stability zone at Hydrate Ridge (Oregon margin): evidence from prolonged degassing of a pressurized core, Earth and Planetary Science Letters, 222, 2004.

Milkov, A. V.: Molecular and stable isotope compositions of natural gas hydrates: A revised global dataset and basic interpretations in the context of geological settings, Organic Geochemistry, 36, 681-702, 2005.

Pape, T., Bahr, A., Rethemeyer, J., Kessler, J. D., Sahling, H., Hinrichs, K.-U., Klapp, S. A., Reeburgh, W. S., and Bohrmann, G.: Molecular and isotopic partitioning of low-molecular-weight hydrocarbons during migration and gas hydrate precipitation in deposits of a high-flux seepage site, Chemical Geology, 269, 350-363, 2010.

Reeburgh, W. S.: Oceanic Methane Biogeochemistry, Chemical Reviews, 107, 486-513, 10.1021/cr050362v, 2007.

Reitz, A., Pape, T., Haeckel, M., Schmidt, M., Berner, U., Scholz, F., Liebetrau, V., Aloisi, G., Weise, S. M., and Wallmann, K.: Sources of fluids and gases expelled at cold seeps offshore Georgia, eastern Black Sea, Geochimica and Cosmochimica Acta, subm.

Ross, D. A., and Degens, E. T.: Recent sediments of Black Sea in: The Black Sea - geology, chemistry and biology, edited by: Ross, D. A., and Degens, E. T., AAPG, Tulsa, USA, 183-199, 1974.

Sloan, E. D., and Koh, C. A.: Clathrate Hydrates of Natural Gases, CRC Press, Boca Raton, 752 pp., 2007.

Tishchenko, P., Hensen, C., Wallmann, K., and Wong, C. S.: Calculation of the stability and solubility of methane hydrate in seawater, Chemical Geology, 219, 37-52, 2005.

Tissot, B. P., and Welte, D. H.: Petroleum Formation and Occurrence, Springer Verlag, Berlin, 1984.

Ussler, W., and Paull, C. K.: Ion exclusion associated with marine gas hydrate deposits, in: Natural Gas Hydrates - Occurrence, distribution, and detection,, edited by: Dillon, W. P., and Paull, C. K., AGU, Washington, DC, 41-51, 2001.

Vassilev, A., and Dimitrov, L.: Spatial and quantity evaluation of the Black Sea gas hydrates, Geologiya i Geofizika, 43, 672–684, 2002.

Wagner-Friedrichs, M.: Seafloor seepage in the Black Sea: Mud volcanoes, seeps and diapiric structures imaged by acoustic methods. , PhD thesis, Department of Geosciences, Univ. of Bremen, Bremen, 154 pp., 2007.

Wallmann, K., Drews, M., Aloisi, G., and Bohrmann, G.: Methane discharge into the Black Sea and global ocean via fluid flow through submarine mud volcanoes, Earth and Planetary Science Letters, 248, 544-559, 2006.

Whiticar, M. J.: Carbon and hydrogen isotope systematics of bacterial formation and oxidation of methane, Chemical Geology, 161, 291-314, 1999.

Table 1. Station information, sulfate depletion depth below core surface and average core porosity.

On Board/Pagea Station Identifier	Location	Latitude	Longitude	Water depth / m	Core length / cm	Sulfate depletion / cm	Average porosity
*BS351AP/*GeoB 9909-2	Batumi	41°57.53 N	41°17.58 E	855	220	25 (50)*	0.721
*BS359AP/*GeoB 9913-5	Pechori	41°58.99 N	41°07.41 E	1031	106	40	0.680
*BS371AP/*GeoB 9923-3	Batumi	41°57.62 N	41°17.52 E	859	175	135	0.705
*BS378AP/*GeoB 9929-2	Batumi	41°57.56 N	41°17.20 E	851	190	50	0.721

* Sediment depth of Core BS351AP was corrected (+25 cm) for porewater data using measurements from video guided multi coring. 220 cm core therefore covers 25-245 cm sediment depth (also see Appendix A).

Tab. 2 – Data from gas collection including volumes of collected gas, CH_4 and gas hydrate as well as dissolved and total CH_4 concentrations in DAPC sediment cores between the depth of sulfate depletion and the core bottom (except BS351AP$^{85\text{-}205cm}$ and BS351AP$^{85\text{-}205,88\%}$).

Station/Core	Core length / cm	Collected gas / L	Air / %	Collected CH_4 / L	ΣCH_4 /mol/kg	ΣCH_4 / mol	$CH_{4\ (aq)}$ / mol	GH* / % pv	GH* / % cv
BS351AP$^{50\text{-}245cm}$	195	226.2	2.24	221.0	1.206	9.03	0.66	14.6	10.5
BS351AP$^{85\text{-}205cm}$	120	226.2	2.24	221.0	1.945	9.03	0.40	24.5	17.7
BS351AP$^{85\text{-}205,88\%}$	120	226.2	2.24	221.0	1.712	9.03	0.40	21.5	15.5
BS359AP	66	88.7	2.53	86.2	1,404	3.52	0.22	17.3	12.3
BS371AP	45	10.9	7.16	10.2	0.234	0.41	0.15	1.9	1.6
BS378AP‡	140	200.6	1.96	196.7	1.425	8.04	0.49	17.6	13.3

*Assuming a molar CH_4/water ratio of 5.9 in sI gas hydrates, i.e. an occupancy of 90% of the small cages by CH_4 (Ussler and Paull, 2001), resulting in 182 L CH_4 per liter of gas hydrate given STP conditions (p = 1013 hPa, T = 298.15 K). (Note: in *Heeschen et al*. (2007) the CH_4 volume of gas hydrate is based on 273.15 K and 164 L). The CH4 equilibrium concentration (C_{eq}) is 0.0087 mol/kg.

‡ A clogged valve let to difficulties while opening the liner which causes higher uncertainties regarding the core length and thus the gas hydrate volume (~ 10%).

Table 3. Average hydrocarbon composition of the collected gas (%) and the Bernard Factor (B_f); n.d. = below detection limit.

Station, Core	C_1 / %	C_2 / %	C_3 / %	i-C_4 / %	n-C_4 / %	i-C_5 / %	B_f
BS351AP	99.966	0.033	0.001	n.d.	n.d.	n.d.	2940
BS359AP	99.634	0.274	0.022	0.055	0.001	0.007	337
BS371AP	99.964	0.024	0.002	n.d.	n.d.	0.007	3845
BS378AP	99.963	0.036	0.001	n.d.	n.d.	n.d.	2701

Table 4. Gas Hydrate Compositions from Batumi Seep Cores (BS350G: n=4; BS352G: n=1) and Pechori Mound (BS356G: n=1; BS360G: n=3); n.d. = below detection limit.

	Batumi Seep		Pechori Mound	
Alkane	*BS350G*	*BS352G*	*BS360G*	*BS356G*
C_1 / %	99.91	99.71	99.14	97.63
C_2 / %	0.08	0.28	0.15	0.25
C_3 / %	n.d.	0.01	0.58	1.64
i-C_4 / %	n.d.	n.d.	0.10	0.39
n-C_4 / %	n.d.	n.d.	0.02	0.08

Figure 1. Working area and coring stations (star symbols and labels) offshore Georgia, eastern Black Sea: A) Detailed bathymetric map of the study area. B) 30 kHz MAK Sidescan sonar mosaic of the Pechori area. C) Detailed 75 kHz DTS-1 sidescan sonar mosaic of the Batumi Seep. The high backscatter intensities in 1B and 1C are shown in light tones and may correlate to the presence of near-surface gas hydrates and authigenic carbonate precipitates [modified after *Klaucke et al.*, 2005].

Figure 2. A) Gas hydrate volumes in shallow sediments of Batumi Seep and Pechori Mound as calculated from the degassing of the DAPC cores, given in per cent pore volume (%pv). Hydrate volumes for core BS351AP are derived from the degassing (gray columns, Gas), the Cl^- profile model in 2B and 2C (black column, Cl) and the volume (black column, comb) gained from the combined results of degassing and the chloride measurements, i.e., 211 L CH_4 locked in gas hydrates at core depth between 85 and 205 cm. B) Measured Cl^- concentrations of BS351AP (dots) in comparison to the modeled 'in-situ' Cl^- profile (Cl_{ref}, dotted line) characterized by the advection of less saline fluids C) Calculated gas hydrate distribution depth as calculated from Cl^- anomalies and Cl_{ref} in core BS351AP. Sulfate depletion in core with BS351AP is reached at 75 cm core depth. See Methods 3.3 and Appendix for details on the model.

Figure A1: Result of the numerical 1-D transport-reaction model (solid lines) of gas hydrate formation in the Batumi Seep Area at Site BS 351 DAPC. Plotted data are a combination of BS 351 DAPC (grey dots) and BS 369 MC (black dots). The DAPC core probably lost ~25 cm sediment at the top, as inferred from the measured porosity data, whereas the multicorer liner penetrated too deep and therefore is missing the top 7 cm of the sediment, as inferred from the sulfate data. The values of the adjusted model parameters of this simulation are given in Table S1. The dotted Cl- profile would be observed ex situ after decomposition of all model-predicted methane hydrate. The dotted porosity profile represents the initial depth distribution without hydrate formation as derived from least squares fitting to the data.

Figure A2: Changes of gas composition (upper 4 panels) and pressure (lower panel) with increasing gas volume during the degassing of pressure core BS351AP. The gray-shaded boxes indicate areas of enhanced compositional changes, possibly due to free gas occurrences (0-11 L and 112-122 L) and porewater degassing (215 – 226 L). See text for further discussion.

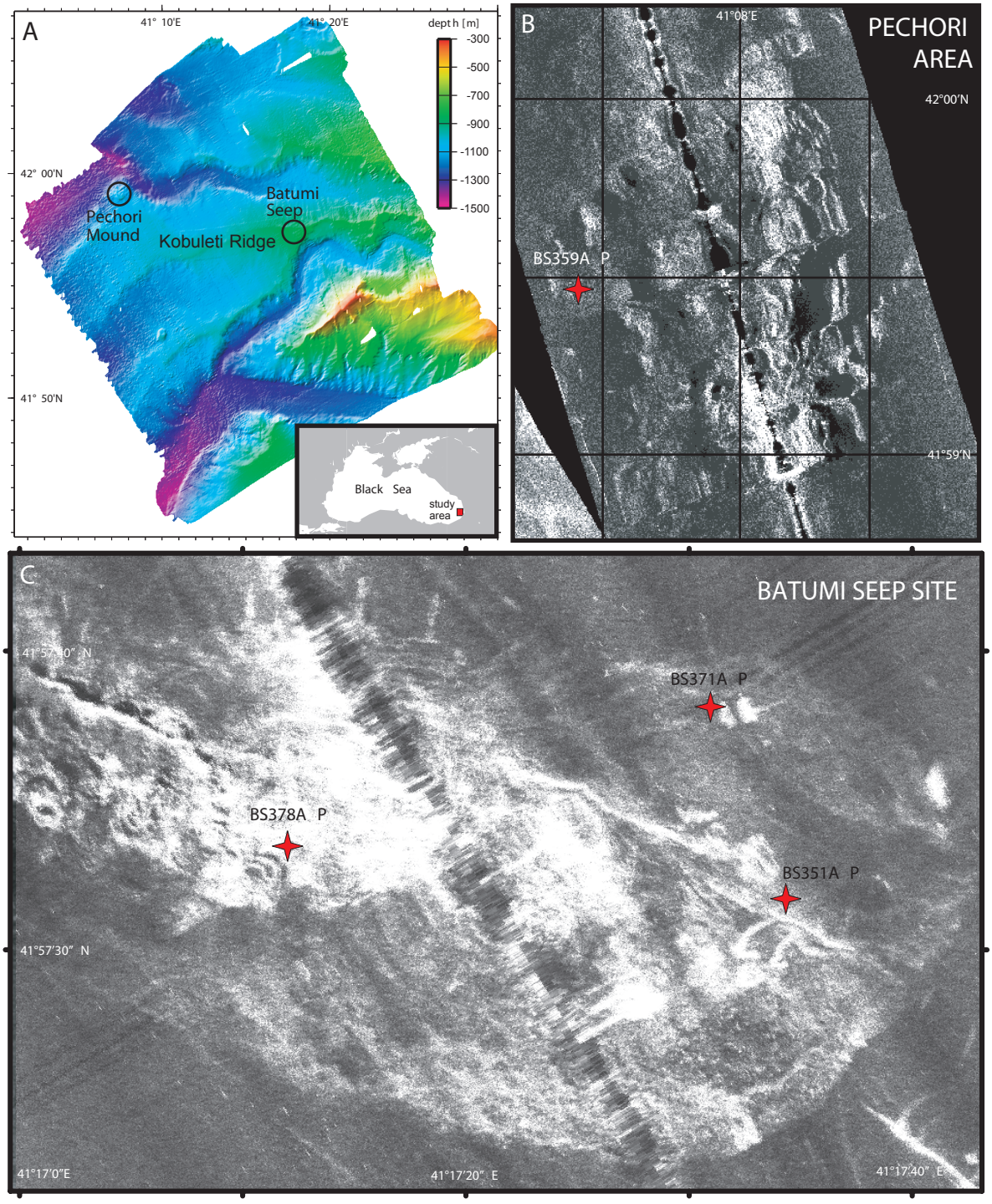
A
41° 10'E
41° 20'E
depth [m]
-300
-500
-700
-900
-1100
-1300
-1500
42° 00'N
41° 50'N
Pechori Mound
Batumi Seep
Kobuleti Ridge
Black Sea
study area
B
41°08'E
PECHORI AREA
42°00'N
BS359A P
41°59'N
C
BATUMI SEEP SITE
41°57'30" N
BS371A P
BS378A P
BS351A P
41°57'30" N
41°17'0"E
41°17'20" E
41°17'40" E

Figure 1

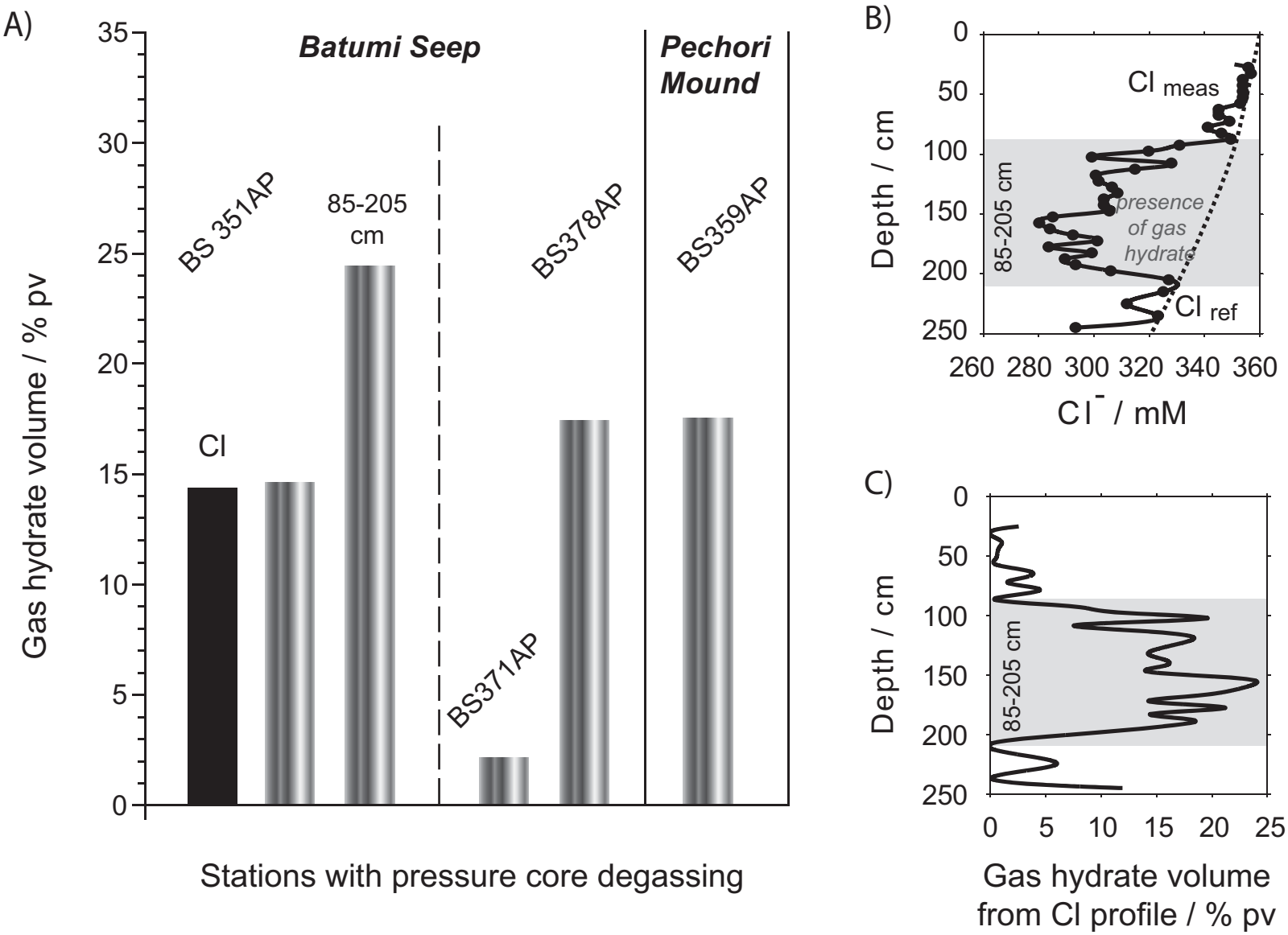
A)
Batumi Seep
Pechori Mound
Gas hydrate volume / % pv
Cl
BS 351AP
85-205 cm
BS371AP
BS378AP
BS359AP
Stations with pressure core degassing
B)
Depth / cm
Cl meas
85-205 cm
presence of gas hydrate
Cl ref
Cl⁻ / mM
C)
Depth / cm
85-205 cm
Gas hydrate volume from Cl profile / % pv

Figure 2

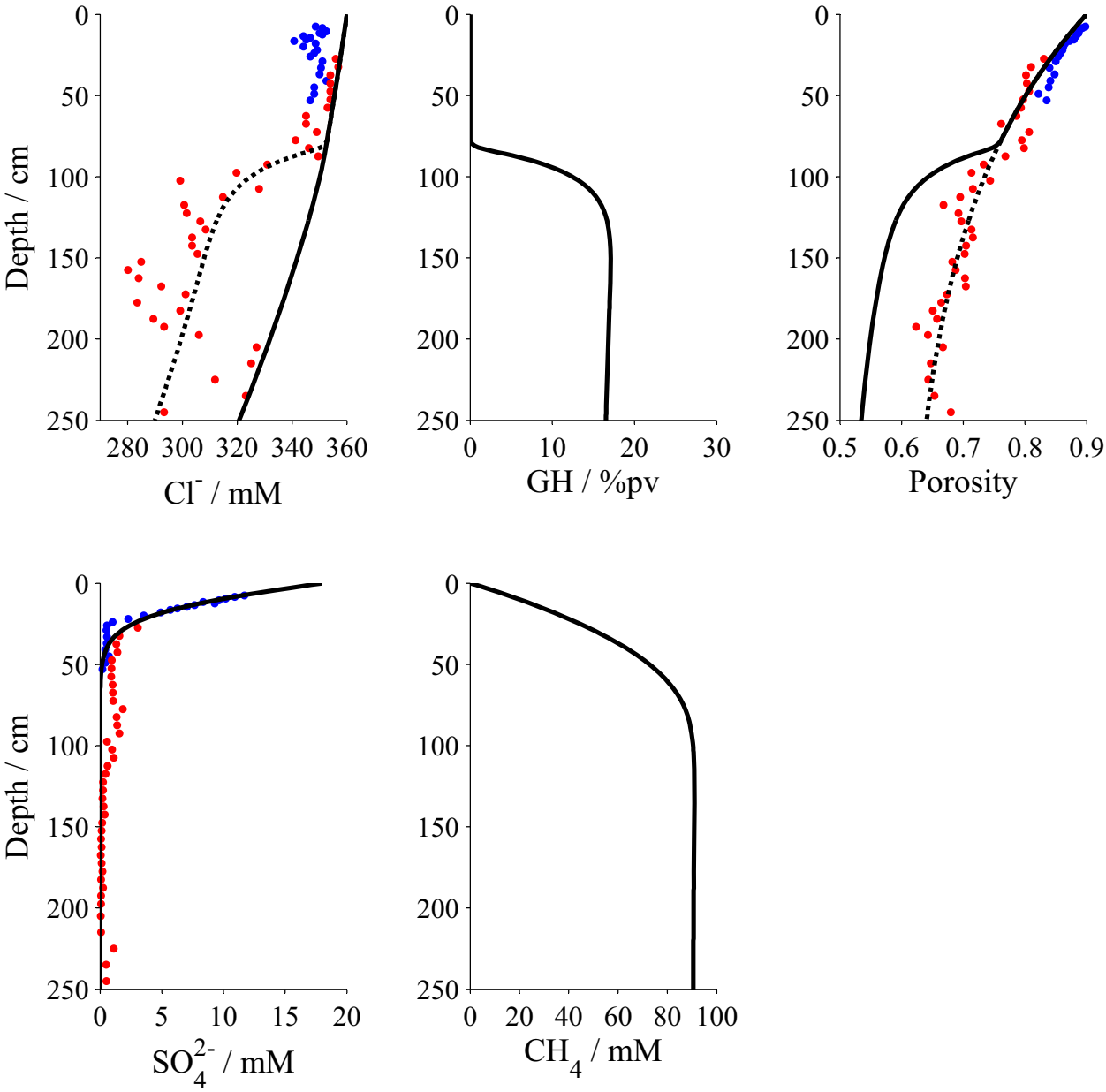
Depth / cm
0
50
100
150
200
250
280 300 320 340 360
Cl- / mM
0 10 20 30
GH / %pv
0.5 0.6 0.7 0.8 0.9
Porosity
0 5 10 15 20
SO4 2- / mM
0 20 40 60 80 100
CH4 / mM

Figure A1

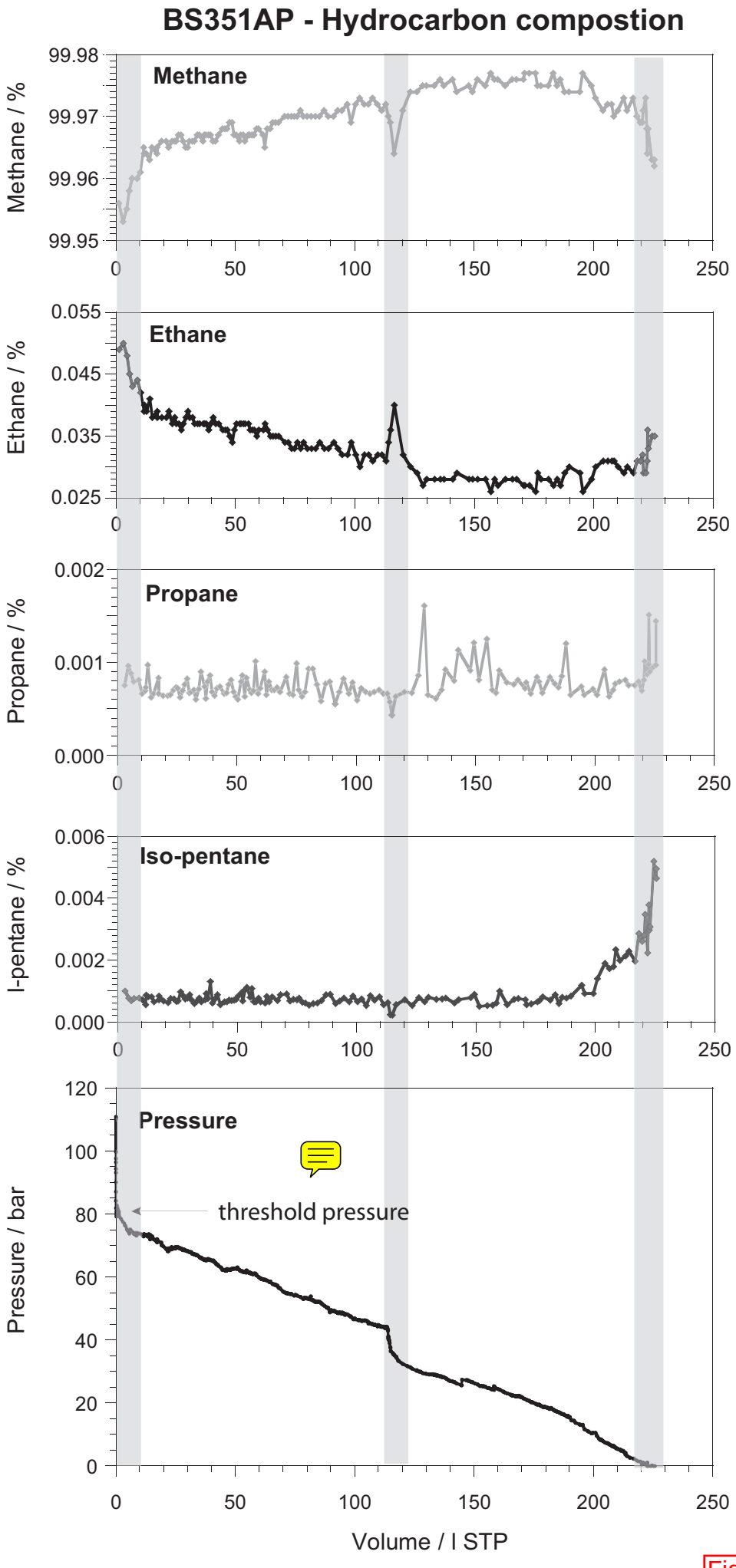
BS351AP - Hydrocarbon compostion
Methane
Methane / %
99.98
99.97
99.96
99.95
Ethane
Ethane / %
0.055
0.045
0.035
0.025
Propane
Propane / %
0.002
0.001
0.000
Iso-pentane
I-pentane / %
0.006
0.004
0.002
0.000
Pressure
threshold pressure
Pressure / bar
120
100
80
60
40
20
0
0
50
100
150
200
250
Volume / l STP

Figure A2